LA-UR -82-1034

MASTER

CONF-820429--2

Los Alamos National Laboratory is operated by the University of California for the United States Department of Energy under contract W-7405-ENG-36.

LA-UR--82-1034

DE82 014083

TITLE: SELF-CONSISTENT ELECTRON TRANSPORT IN COLLISIONAL PLASMAS

AUTHOR(S): Rodney J. Mason

SUBMITTED TO: Los Alamos/CEA Applied Physics Conference, Paris, France, April 19-23, 1982

Los Alamos Los Alamos National Laboratory
Los Alamos, New Mexico 87545

FORM NO 836 R4
ST NO 2629 5/81

SELF-CONSISTENT ELECTRON TRANSPORT IN COLLISIONAL PLASMAS*

Rodney J. Mason
Los Alamos National Laboratory
Los Alamos, New Mexico 87545

A self-consistent scheme has been developed to model electron transport in evolving plasmas of arbitrary classical collisionality. The electrons and ions are treated as either multiple donor-cell fluids, or collisional particles-in-cell. Particle suprathermal electrons scatter off ions, and drag against fluid background thermal electrons. The background electrons undergo ion friction, thermal coupling, and bremsstrahlung. The components move in self-consistent advanced E-fields, obtained by the Implicit Moment Method, which permits $\Delta t \gg \omega_p^{-1}$ and $\Delta x \gg \lambda_D$ -- offering a 10^2 - 10^3-fold speed-up over older explicit techniques. The fluid description for the background plasma components permits the modeling of transport in systems spanning more than a 10^7-fold change in density, and encompassing contiguous collisional and collisionless regions. Results are presented from application of the scheme to the modeling of CO_2 laser-generated suprathermal electron transport in expanding thin foils, and in multi-foil target configurations.

---

*This work was performed under the auspices of the United States Department of Energy.

SELF-CONSISTENT ELECTRON TRANSPORT IN COLLISIONAL PLASMAS

INTRODUCTION

At laser wavelengths of 1 μm and above a significant fraction of the light absorbed by laser fusion targets is deposited in suprathermal electrons. These are marginally collisional and distribute the absorbed energy throughout the target. As they move they set up self-consistent E-fields, which draw return currents in the background, generally strongly collisional, thermal electrons. These fields also set the ions into motion, changing the target geometry, in which the suprathermals must transport. A detailed model of this complex coupled phenomenology is required, if we are to develop the intuition and understanding needed to engineer the use of suprathermals in the design of targets for high compression. Thusfar, our efforts toward the development of such a model have been confined to a one-dimensional treatment. However, our choice of approach has been guided by the ease with which it might be generalized to higher dimensions.

Thus, we treat the suprathermal electrons as collisional particles-in-cell. The Particle-in-Cell (PIC) approach[1] has established reliability in application to collisionless modeling in one and two dimensions. Motion in self-consistent fields presents no difficulty. The weak effects of ion scatter and electron drag are readily added with the inclusion of simple operators on the suprathermal velocities. The return current thermal electrons are moved as a collisional donor-cell fluid. This allows us to treat the very large range of background densities from solid and above down through critical and into the corona. The resistive force between the thermals and ions is handled implicitly, so strong collisionality simply leads to low relative drift speeds. The fluctuations of a particle background representation are avoided. Similarly, a donor-cell Eulerian treatment of the ions allows for the efficient treatment of the ion hydrodynamics. Flux-correction and gating of the hydrodynamics at vacuum boundaries is employed to reduce numerical diffusion. The electrons and ions move in a self-consistent E-field calculated by the Implicit Moment Technique. For this an auxillary set of fluid equations is solved implicitly with the Poisson equation to give an advanced field. By moving the electron and ion components in this field, we avoid the usual time-step constraint to steps less than the minimum plasma period. Thus, global problems spanning a large density range can be run as much as a thousand times faster than by traditional explicit methods.

The collisional PIC treatment for the suprathermals has been previously outlined in Refs. 2 and 3. Dawson and Shanny[4] were the first to use the electron-ion scattering procedure. A rudimentary form of the Implicit Moment Technique for the E-field is found in Ref. 2. We provide a more rigorous and complete discussion in Ref. 5. For the fluids we followed the donor-cell prescription given by Gentry et al.[6], with flux-correction improvements, as recommended by Boris et al.[7], and Zalesak[8].

Although a multi-group treatment of the suprathermals would be computationally more efficient, we avoid it to skirt the need for suprathermal flux-limitation in collisionless regions, and anticipating later difficulties in extending a self-consistent multi-grup treatment to higher dimensions. Forslund and Brackbill[9] have shown that Implicit Moment Particle Simulation readily extends to two-dimensions. An Eulerian description was chosen for the fluids to provide compatibility with the field and particle descriptions on a fixed orthogonal mesh. The price for this convenience was found to be severe numerical diffusion at the vacuum boundary of a laser target. We found that a density triggered gate, essentially making the outer boundary a Lagrangian zone, was suffucient to terminate this diffusion. An advantage of the gate is that it in no way limits time steps in the accurate modeling of suprathermal-driven fast ion blowoff.

In the next section of this paper we will detail the important and crucial features of our computational model. The collisional PIC suprathermal approach will be reiterated. The modifications in the standard donor-cell procedures needed to allow for two-fluid collisional hydrodynamics (colliding thermal electrons and ions) will be stressed. Also, we will focus on the changes in the Implicit Moment Technique demanded by the presence of collisions and the simultaneous use of both particle and fluid hydrodynamic descriptions for the plasma components. Then, in the following section we will demonstrate application of the net transport scheme to the motion of suprathermals through thin and thick single foils, as well as double foil target configurations, as might be used for vacuum insulation. The concluding section will sumarize our findings, and recommend future directions.

THE COMPUTATIONAL MODEL

SUPRATHERMAL ELECTRON PARTICLES

Emission and Motion

The modeling begins with an initially prescribed background plasma of thermal electrons and ions. These are described on a one dimensional mesh of typically 100 cells. At some prescribed location suprathermal (or hot) electrons are emitted. This location is preset for certain test problems or chosen by operations which follow laser light up to the critical surface, which then becomes a moving emission point for the hots. As the hot electrons are produced, the background density of thermal (or cold) electrons is correspondingly reduced. When the hot emission is meant to mock-up resonance absorption, the electrons are given a drifting Maxwellian distribution in a 20^{o} cone about the direction towards the laser. They thus will move with a longitudinal velocity u and carry a transverse velocity component v_t. Their temperature T_h is given by Forslund's formula[10], $T_h \sim (I\lambda)^{1/3} T_c^{1/3}$, in accordance with experiment and theory. For certain tests the dependence on the cold background temperature T_c may be neglected, or T_h may rimply be fixed.

Typically, two electrons are emitted each computational cycle. Their velocities are changed by drag and scattering operators, and then they are moved according to

$$u^{(m+1)} = u^{(m)} + \frac{q_\alpha E^{(*)}}{m} \Delta t \quad , \tag{1a}$$

$$x^{(m+1)} = x^{(m)} + u^{(*)} \Delta t \quad , \tag{1b}$$

Here $u^{(*)}$ and $E^{(*)}$ are appropriately centered choices for the drift velocity and field. At present to insure the greatest numerical stability and simplify the model, for (*) we use level (m+1).

Drag

Coulomb drag slows the suprathermals against the background electrons. To model this we reduce the hot speeds each cycle by

$$\Delta c = \frac{-4\pi e^4 n_i}{mkT_e} \Delta t \; G(\xi) \; \log \lambda \quad , \quad \xi = \left(\frac{mc^2}{2kT_e} \right)^{1/2} \quad , \tag{2a}$$

in which

$$G(\xi) = \frac{0.376 \, \xi}{(1 + 0.542 \, \xi - 0.204 \, \xi^2 + 0.752 \, \xi^3)} \tag{2b}$$

is a polynomial fit to Spitzer's error function combination[11], and $c^2 = u^2+v^2$. Thus, the drag goes as c^{-2} for large speeds, as in Ref. 2. It peaks at $\xi=1$ and is zero as $c \to 0$. Energy dragged from the suprathermals is redeposited locally in the thermals, raising T_c. At present the lost momentum is discarded. To avoid unphysical thermal heating as the hot electrons reflect in the corona, the drag is supressed for $n_h > n_c$. Otherwise, when the energy of a hot electron is dragged below kT_c the slow hot electron is destroyed, with its density and energy attributed to the thermal electron background. In sufficiently collisional problems a semi-equilibrium situation can be established, in which the hot electrons created by the resonant absorption process are eventually all destroyed by

the drag, and the number of simulation particles needed to describe the suprathermals in flight is relatively constant.

Scatter

It is assumed that each hot electron undergoes many small angle deflections on crossing a finite thickness of plasma. Since the successive collisions are independent events, the central limit theorem indicates that for Rutherford scattering, the distribution $P(\theta)$ of net deflection angles, $\theta > 0$ from the original forward direction for each electron, will be approximately Gaussian[2,4], i.e.

$$P(\theta) = \frac{\theta}{\langle\theta^2\rangle} \exp\left(\frac{-\theta^2}{2\langle\theta^2\rangle}\right) \qquad (3)$$

with $\langle\theta^2\rangle = 8\pi e^4 m^{-2} c^{-3} \Delta t n_i Z(Z+1) \log\lambda$. In the Z+1 factor the Z accounts for scatter off ions and the +1 term approximates the effect of scatter off electrons. In each time step random numbers are picked from a list of 10^4 preestablished random numbers and used to pick a new θ and a new uniformly distributed azimuthal angle ψ. The use of this random list speeds the angular selection process by a factor of about three at the cost of minor error in the randomness. Overall in a scattering event the velocity vector of a suprathermal is simply rotated, and its energy is conserved. The trigonometry associated with these rotations is detailed in Ref. 2. When the background density is sufficiently low or an electron is sufficiently energetic, $\langle\theta^2\rangle \ll 1$, and the electron is essentially undeflected during a time step. There is also minimal drag so that its motion is essentially that of conventional fully-deterministic PIC.

On the average, this scattering procedure gives an effective collision frequency for the suprathermals of $\nu = \langle\theta^2\rangle/(2\Delta t)$, where ν is the rate of mean momentum loss from friction against the ions and background electrons. As formulated, our scattering procedure is valid only so long as $\nu\Delta t < 1$. For longer time steps the particle motion should become a random walk, with the total distance traversed during a time step significantly reduced below $v\Delta t$. Some progress has been made in limiting the particle excursions to the limits imposed by Brownian motion[3], but for the present model we choose instead to treat the more collisional electrons as a thermal fluid. Conversion of the more collisional hot electrons to thermals in the drag modeling generally obviates the need for scrutiny of the $\nu\Delta t < 1$ requirement in the application of the model to CO_2 generated suprathermal transport.

THERMAL ELECTRON AND ION FLUIDS

A fluid treatment is needed for the background plasma in order to model strongly collisional regions, but also to manage the very large range of densities encountered in laser-target simulations. When 100 particles/cell are used to represent the peak density region of a foil, the lowest density resolvable is 1/100 th of the peak. Fully ionized gold at solid density represents about 4×10^{24} electrons/cm^3 so with this small simulation particle density, only regions down to 4×10^{22} could be explored, while the critical density for CO_2 is 10^{19} cm^3, and modeling of transport in the contiguous solid and critical regions could prove crucial to important pellet designs. This limit to resolution presents no difficulty in the hot electron modeling, since the order of 10^{19} hot electrons/cm^3 are established, and there is little need to model them in regions where their density drops below 10^{17}.

We use an extention of Braginskii's equations[12] for the two-fluid background plasma. For fixed ions this extension is given in Refs. 2. We solve the fluid equations using a variation on the donor-cell procedure of Gentry et al.[6]. At each time step the hydrodynamics is divided into a "Lagrangian" and then an "Advection" phase. During the Lagrangian phase the fluid velocities are advanced by the local pressure gradients and E-fields. The resistive terms in the momentum equations are treated implicitly, so that strong collisions directly implies diffusion of the cold thermals through the ions. Similarly, during this phase the fluids undergo PdV work and the electrons acquire joule heating and deposited energy from the dragged suprathermals. We store the cold electron and ion densities, velocties and temperatures $n_{c,i}, u_{c,i}$ and $T_{c,i}$ at the computational cell centers. During the Advection phase this information is convected to neighboring cells.

When the ions can move, the thermal electrons should drift at the local ion speed in strongly collisional regions. Thus, for the differenced coupled momentum equations we use

$$j_{h,c}^{(m+1)} = j_{h,c}^{(m)} - \frac{1}{m}\frac{\partial \Pi_{h,c}^{(m)}}{\partial x}\Delta t - \frac{e n_{h,c} E^{(m+1)} \Delta t}{m}$$

(4a,b)

$$- \nu_n \Delta t \left(j_{h,c}^{(m+1)} - \frac{n_{h,c} j_i^{(m)}}{n_i} \right)$$

$$j_i^{(m+1)} = j_i^{(m)} - \frac{1}{M}\frac{\partial P_i^{(m)}}{\partial x}\Delta t + \frac{Zen_i E^{(m+1)}\Delta t}{M}$$

(4c)

$$- \left(\nu_H \Delta t \frac{n_h}{n_i} + \nu_c \Delta t \frac{n_c}{n_i}\right) \frac{m}{M} j_i^{(m)} + \nu_H \Delta t \frac{m}{M} j_h^{(m+1)} + \nu_c \Delta t \frac{m}{M} j_c^{(m+1)}$$

when thermoelectric effects[2] are neglected. Here Π is the total pressure $\Pi \equiv n(mu^2+kT+)+P_a$, and, of course, $j \equiv nu$; P_a is a Von-Neuman artificial viscosity. The j_h equation is, for the most part, redundant, being used here to render explicit the information needed in collision term for the ion momentum equation. The level (m) hot electron moment data is obtained from PIC accumulations. The collision rates $\nu = 1/\tau$ are from Braginskii, as in Ref. 2 with $T \rightarrow (T+mu^2/3k)$, including the u^2 to approximate the effect of large drift velocities. The j_i elements in the collision terms are left at level (m) to simplify the algebra in the solutions for $j_{c,i}^{(m+1)}$. This restricts the model to moderately collisional regimes, such that the product $\nu\Delta t\ m_e/M << 1$.

For the Lagrangian phase of the hydrodynamic calculation we solve Eq.(4) for $j_{c,i}$. The mu^2 terms are suppressed in Π during this phase, but the artificial viscous pressure is retained. In the $\nu\Delta >> 1$ limit the solution to Eq.(4) for j_c becomes

$$j_c^{(m+1)} = -\frac{1}{m\nu_c}\frac{\partial \Pi_c^{(m)}}{\partial x} + n_c u_i^{(m)} - \frac{en_c E^{(m+1)}}{m\nu_c} \qquad (5)$$

which is equivalent to an Ohm's law. This will let u_c differ from u_i as a result of particle diffusion or an external electric field.

The advection is carried out by first defining average velocities at the cell boundaries, u(i+1/2)=0.5*(u(i)+u(i+1)), and then by fluxing n, nu and nT across these boundaries from the donating cells, as determined by the sign of u(i+1/2). Thermal energy kT is fluxed, rather than total energy, to improve the accuracy of the T determinations (upon which resistivity strongly depends) at the expense of accuracy in the energy conservation. The fluxing is then followed by an anti-diffusive flux corrective calculation[7,8] to sharpen the fluid profiles. This substitutes a second order, essentially Lax-Wendroff solution for the first order (in space) donor-cell solution, wherever this can be done without producing non-physical maxima in the results.

We found that the Eulerian fluid calculations did a poor job of modeling the adiabatic expansion of foils, even with the addition of the FCT anti-diffusive corrections[7,8], until gating of the vacuum boundary was introduced. Eulerian calculations tend to diffuse information across a mesh at a rate of one cell/cycle. This can manifest itself as a persistence of high material temperatures at the edges of an expanding flow (essentially the initial temperatures) where $T \sim n^{2/3}$ should be expected. There can also be extreme temperature spikes at the edges, as the calculations effectively register shock heating of the vacuum. An extrapolation of the cell-centerd velocities out into the vacuum[13] was found to eliminate most of the spike (by supressing any PdV heating there). Then, the implementation of FCT[7,8] was found to stop most of the numerical diffusion of temperature. Remaining small edge spikes in n and T were removed by the gating operation which set the edge velocity to zero until the density behind it reached a value extrapolated from the interior of the material. Note that for two-temperature expansions, in which hot electrons drive the expansion of a low density fast ion edge, the gate opening must depend on an extrapolation of the hot electron density.

In dense collisional regions the thermal electron and ion temperatures will equilibrate; there will also be some radiative emission. We model this by coupling T_c to T_i at the Spitzer[14] rate, following the hydrodynamic advancement of the fluids, and by decrasing T_c as a bremsstrahlung loss, limited locally to the blackbody emission rate.

THE IMPLICIT MOMENT E-FIELD

Traditionally, a solution for the E-field through tne Poisson equation would restrict calculations to time steps less than the minimum local plasma period on the simulational mesh. We surmount this problem by the Implicit Moment Method[5], by which we introduce auxiliary fluid equations which are solved in conjunction with the Poisson equation for the advanced field $E^{(m+1)}$. Explicit particle and fluid advances are stable in the advanced field for time steps constrained only by a Courant condition on the hottest electrons[5,9]. For global problems this procedure permits time steps typically 10^3 times larger than those required by earlier methods.

Thus, integrating the Poisson equation in space for time level (m+1)

$$E^{(m+1)} = 4\pi \int_0^x \sum_\alpha q_\alpha \tilde{n}_\alpha^{(m+1)} \, dx + E^{(m+1)}(0) \qquad (5)$$

and obtaining densities $\tilde{n}_\alpha^{(m+1)}$ by integrating the continuity equation in time for each spiecies, i.e.

$$\tilde{n}_\alpha^{(m+1)} = n_\alpha(m) - \frac{\partial}{\partial x}\left(j^{(m+1)}\right)\Delta t \quad , \tag{7}$$

we employ the advanced currents $j_\alpha^{(m+1)}$ from the solutions to eqs. (4), and obtain

$$E^{(m+1)} = \frac{4\pi\left\{\int_0^x \sum q_\alpha n_\alpha^{(m)} dx + I\Delta t + \sum \frac{c_\alpha q_\alpha}{m_\alpha}\frac{\partial \Pi_\alpha^{(m)}}{\partial x}(\Delta t)^2\right\}}{(1+\omega_p^{\sim 2}(\Delta t)^2)} \tag{8a}$$

for the E-field, when $E(0)=j_\alpha=0$ -- as for a quiescent left boundary. Here

$$\omega_p^{\sim 2} \equiv \frac{4\pi e^2}{m}\left(n_h c_h + n_c c_c + \frac{Z^2 m}{M} c_i n_i\right) \tag{8b}$$

and

$$c_i \equiv 1 - \left[(\nu_H \Delta t)c_h + (\nu_c \Delta t)c_c\right]/Z \tag{8c}$$

$$c_h \equiv \frac{1}{1+(\nu_H \Delta t)} \quad , \quad c_c \equiv \frac{1}{1+(\nu_c \Delta t)} \quad . \tag{8d,e}$$

Also,

$$I \equiv j_h^{(m)} c_h + j_c^{(m)} c_c - ZJ_i \tag{8f}$$

and

$$J_i = j_i^{(m)} \left[1 - \frac{m}{M}(\nu_h + \nu_c)\Delta t\right] + g_h^{(m)} c_h(\nu_H \Delta t) + g_c^{(m)} c_c(\nu_h \Delta t) \qquad (8g)$$

in which, finally,

$$g_{h,c} = j_{h,c} - \frac{1}{m}\frac{\partial \Pi_{h,c}}{\partial x}\Delta t \quad . \qquad (8h)$$

Furthermore, (q_α, m_α) are $(-e,m)$ for the electrons and (Ze,M) for the ions. In the collisionless limit this becomes

$$E^{(m+1)} = \frac{4\pi\left\{\int_0^x \sum q_\alpha n_\alpha^{(m)} dx - \sum q_\alpha j_\alpha^{(m)}\Delta t + \sum \frac{q_\alpha}{m_\alpha}\frac{\partial \Pi_\alpha^{(m)}}{\partial x}(\Delta t)^2\right\}}{(1 + \omega_p^{-2}(\Delta t)^2)} \qquad (9)$$

in which,

$$\omega_p^{-2} = \frac{4\pi e^2}{m}\left[n_e + \frac{m}{f} Z^2 n_i\right] \quad .$$

In quasineutral regions, where $\omega_p^2 \Delta t >> 1$, and when $m/M << 1$, eq. (9) reduces to $E = -1/en_e \partial P_e/\partial x$, where $n_e = n_h + n_c$ and $P_e = P_h + P_c$, plus the summational density and current "correction" terms, which help to maintain the charge neutrality. Alternatively, when $\omega_p^2 \Delta t << 1$ the field reduces to the Poisson result of the integral over the sum of the old charge densities $q_\alpha n_\alpha^{(m)}$.

In dense collisional regions eq. (8) essentially reduces to eq. (5), the Ohm's law. Furthermore, by quasi-neutrality $j_c = j_h$, so that in dense interior regions of a target where the hot electrons are essentially undeflected by collisions or the fields, $j_h^{(m+1)} = j_h^{(m)}$, and thus through eq.(5) the E-field is determined essentially from the old hot current.

The full E-field equation, eq. (8), is basically eq. (24) of the Moment Method of Ref. 2, except that charge separation effects are now retained, as a result of using the continuity equations, eq. (7). The

collisionless result has been given in Ref. 5 and explored by Denavit in Ref. 15. Its extention to two-dimensions is accomplished in Ref. 9.

In the auxiliary fluid equations for the E-field solution, eqs. (7 and 8), we retain the dynamic pressure contributions $m_\alpha n_\alpha u_\alpha^2$ at the old time level (n). This allows us to get the field solution by a simple algebraic rearrangement of the equations. On the other hand, this name term must be extracted and treated in the separate advective stage of the thermal electron and ion advancement schemes in order to assure hydrodynamic stability. Moreover, at the vacuum edge of the fluid the advection must be done by the donor-cell technique, i.e. material must be drawn from the donating cell established by the cell's boundary velocity, so as to assure positivity of the fluid number densities. When the hot electrons enter a boundary region for example, the resultant E-field will draw the cold electrons out, and their density must go no lower than zero. This positivity is guaranteed by the donor-cell hydrodynamics. However, a corresponding careful use of donor-cells in the auxiliary hydrodynamic equations for the E-field solution would mean that the mnu^2 terms would not be known until E itself was known, and this would clearly require iteration to solve for E. By using the old dynamic pressures we find such iteration to be unnecessary. The resultant slight difference in the hydrodynamic equations used for E and in the hydrodynamic procedure then used for the actual fluid advance appears to cause no non-physical consequences. A very similar incompatibility exists in the fluid equations used to represent the hot electrons in the E-field solution and the set of particle equations actually used to advance the hot electron properties. The fluid equations can be goiffured to closely to mimic the motions of the particles on the average[9], but the agreement is never perfect, nor has this proven to be necessary.

THE MULTI-FLUID HYBRID APPROACH

The net system derived for transport studies has great versatility. For tests the hot emission can be supressed, the thermal electron-ion thermal coupling can be skipped, and the E-field and scattering rate can be set to zero. Then in foil geometries, for example, the thermal electron and ion fluids expand entirely separately. If the ion mass is made artificially equal to the electron mass (by setting a single code parameter) the two fluids expand in superposition -- all their properties are identical. At the physical mass ratio the electron expansion is well ahead of the ion expansion, until the scattering or field are restored. When just the scattering is "on" the electrons are locked into motion with the ions, except at the leading edge of the expansion, where they can diffuse ahead. With the field "on" the electrons and ions expand together at the ion acoustic rate[16]. Restoration of the electron-ion thermal coupling gives the ions and cold electrons equal temperatures in dense regions. Finally, when hot emission is "on" the hot electrons interchange with the colds during the net expansion, and joule heating of the thermals is evident. The aim of the modeling is to study this highly coupled phenomenology in evolving one-dimensional geometries.

APPLICATIONS

TEST RUNS

Figure 1 collects results from a number of test runs with the model. Suprathermals were introduced at the vertical fiducial into fixed ion density profiles as depicted in frame (c). For clarity of exposition the electrons were emitted as a left-travelling beam moving at 75 μm/ps. This corresponds to an energy of about 25 keV. The electrons must move through a plateau region where the background density is 10^{20} cm^{-3} into a slab region about 50 μm wide where the peak density is 10^{22} cm^{-3}. In the frame (a) calculation the suprathermals experience only drag, which reduces their speeds as they pass through the dense region. The left boundary is a mirror. Frame (b) shows the effects of both drag and scatter on the high energy particle electrons. The magnitude of the mean drift speed to the left is reduced, as with the drag alone, and a significant fraction of the incident beam has its u component of velocity reversed by the scatter. Finally, frames (c) and (d) show the cumulative effect of drag, scatter and E-field accelerations. The emission point and fiducial have been shifted to the 160 μm position. Frame (c) shows the hot density n_h, and a cold density n_c noticeably below Zn_i in the plateau region. The phase plot of frame (d) shows that the incident beam is coupled to the returning stream of background thermals by a two-stream instability in the first 30 μm of plateau region plasma. More generally, when the incident hot stream is less beamlike and closer to a Maxwellian with a temperature near the drift energy, two-stream effects are much less evident. Also, as the mean particle energy is raised appreciably beyond 25 keV, the localized effects of drag and scatter are much less discernable.

THIN AND THICK FOILS

Figure 2 shows the results for a foil illuminated by CO_2 light at a constant intensity of 3×10^{15} W/cm^2. We deposit 35% of this light and reflect the rest. The light enters from the right and deposits in the first cell with a density exceeding critical, i.e. where $Zn_i > 10^{19}$. The background temperature for thermal electrons and ions is initialized at $T_c = T_i = 1$ keV. The resonance absorption hot emission temperature for these conditions is about 35 keV; T_h has been fixed at this value.

The foil is 9.6 μm thick (4 cells) and made of gold. We assume full ionization and set Z = 79. Thus, the peak thermal electron number density Zn_i is 3.95×10^{24}. The thermal electron-ion coupling is very strong, such that $T_c = T_i$ in the center of the foil throughout the various runs. The proton-electron mass ratio has been artificially set to 10^2, instead of 1836, to economize and speed the evolution of the ion hydrodynamics.

Frames (a) and (b) are for scattering and drag "off", but the E-field "on". Here the vertical fiducial tracks the location of the critical surface. Frame (b) shows that by 5.8 ps the hot electrons have initiated fast ion blow-off on both sides of the foil. This early blow-off has moved nearly twice as far on the laser side. The fast ion density tracks the density of the hot electrons, which peaks at over 10^{20} cm^{-3}, or ten times critical, in

the center of the foil. Thermal electrons are strongly excluded from the fast ion regions. These electrons do drive a slow expansion of the main body of the foil, however, so that the $Zn_i = 10^{20}$ cm^{-3} points have have moved some 20 μm from their initial positions.

In the run for frames (c) and (e) we have turned on the scatter as well as the E-field. The density of the 35 keV suprathermals then drops by more than a factor of ten across the foil. From the phase plot (e), it is evident that the scatter is still holding most of the suprathermals on the laser side of the foil at t = 5.8 ps. Some have penetrated, however, to initiate a fast ion expansion, peaking at $Zn_i = 10^{19}$ cm^{-3} on the back side. Frames (d) and (f) show the results at the same time, 5.8 ps, when the effects of drag on the suprathermals are included. In this case the suprathermals are totally confined to the laser side of the foil. The phase plot shows a significant reduction in the number of particle hot electrons, since many have been slowed to low speed and absorbed in the background. Relatedly, the number with negative, foil-entrant u-components significantly exceeds the number with u > 0.

It is important to note, that in all three runs with 35 keV suprathermals, the critical surface at late time lies well out in the corona, where there are no thermal electrons. Thus, strictly speaking, there are no colds to be heated. This means that we have assumed a hot temperature that is unrealistically low. The model presently manages this situation by reducing the weights of the local suprathermals at critical to conserve charge, as it emits new suprathermals. However, since the emission temperature and energy are fixed, energy is not conserved. In a later version of the model, the emitted hots will be given a higher temperature to account for the energy born by the colder suprathermals they replace. For the present, however, we correct the deficiency in subsequent examples by going to markedly higher emission temperatures than suggested by the resonance absorption formula[10]. This need for higher temperatures is consistent with recent CO_2 experiments.

150 KEV TRANSPORT

The emission temperature was raised to 150 keV for the Figure 3 run, while the foil thickness was reduced to 4.8 μm (2 cells), and its initial temperature was decreased to 1 eV. We continue to assume full ionization, Z=79, for simplicity, although a more comprehensive treatment, in which Zn_i would start at low values and come up as T_c rose, is certainly desireable and planned for future studies. The lower T_c markedly increases the initial resistivity of the foil. However, frame (c) shows that the drag deposition and joule heating effects rapidly raise the coronal thermal and ion temperatures to the 100 eV range, reducing this resistivity.

Frame (a) verifies that with the higher T_h the critical surface shifts left to rest on the cold electrons, and the hot density is substantially reduced to levels below about 10^{19} cm^{-3}. The calculation now consistently converts the colds to hot electrons. Frame (b) shows that a potential the order of $3T_h$ develops to maintain the quasineutrality of the system. It also displays the active E-field in relative units. The phase plot (b), and

also the n_h profile in (a), demonstrate that the E-field does act with some success to constrain the hot electrons to the laser side of this thinner foil. Frame (c) verifies that T_h ranges between 100 and 200 keV across the foil.

The inhibiting effect of resistivity in the cold central region of the foil is less than anticipated, and will be explored more carefully with finer zoning, for example, in future work. Evident, here, however, is the fact that the very energetic electrons present in the tail of a 150 keV suprathermal spectrum can penetrate very large resistive potentials, indeed, while eventually reflecting off the sheaths of a foil. Their return motions after these reflections can then cancel much of any hot directed drift current through resistive barriers, leading subsequently to a lowering of such barriers.

TWO-FOIL VACUUM INSULATION

As a final application of the model, we discuss the closure of a vacuum gap between two foils. In Figure 4, to the foil previously discussed, we add a second identical foil separated by 60 μm. The laser illumination conditions are unchanged. Frame (c) shows the gap between the foils is still open at 1.4 ps, while it closed in frame (e) at 5.2 ps (this takes about 25 ps at the physical m_e/M). In fact, there is then little difference between the n_h profile with or without (as in Fig. 3) the presence of the second foil. We had anticipated the possible development of potential barrier to the hot electrons, as they first began to penetrate the second foil. This is not in evidence, again possibly due to the very long range for the 150 keV suprathermal tail. A reexamination with finer zoning and a T_c dependent Z is needed here too.

CONCLUSIONS

A hybrid electron transport model has been outlined, in which collisional-PIC suprathermal electrons are moved self-consistently through background fluids of mutually colliding thermal electrons and ions. Implicit E-fields, permitting economical calculations are obtained by the Implicit Moment Method. The particle description for the suprathermals assures the adequate modeling of effects dependent on the detailed hot electron distribution. The directions to be followed for an eventual two-dimensional generalization of this description are also quite clear, particularly from the work of Brackbill and Forslund. The addition of fluid ion and thermal electron treatments allow for modeling over the full range of background densities required for global pellet simulations.

The utility of this approach has been demonstrated with applications to CO_2 generated transport in simple foil geometries. An immediate outgrowth of these applications is the result that the moderate suprathermal electron temperatures anticipated with resonant absorption are too low to allow for the self-consistent conversion of cold background thermal electrons into suprathermals. This difficulty is eliminated with O(150 keV) suprathermal

emission, in consistency with recent CO_2 experiments. Simulations run with these hotter suprathermals show them to be extremely penetrating, and apparently capable of closing the gaps in vacuum insulation with no anomalies. This, however, is inconsistent with recent experimental data which now suggests some considerable inhibition of the suprathermals. Thus, more detailed application of the model, with, for example, much finer zoning, and improved ionization physics, is in order, as is a two-dimensional generalization to explore the effect of B-fields in the presence of thermal electron resistive effects.

REFERENCES

1. R. L. Morse, in "Methods of Computational Physics", edited by B. Alder, B. Fernbach and M. Rotenberg (Academic, New York, 1970), Vol. 9, p. 213.

2. R. J. Mason, Phys. Fluids 23, 2204 (1980), and Phys. Rev. Lett. 43, 1795 (1979).

3. R. J. Mason, in "Proceedings of the ANS/ENS International Topical Meeting on "Advances in Mathematical Methods for Nuclear Engineering Problems", Munich, W. Germany, April 27-29,1981.

4. R. Shanny, J. M. Dawson and J. M. Greene, Phys. Fluids 10, 1281 (1967), and Phys. Fluids 12, 2227 (1969).

5. R. J. Mason, J. Comp. Phys. 41, 233 (1981).

6. R. A. Gentry, R. E. Martin, and B. J. Daly, J. Comp. Phys. 1, 87 (1966).

7. D. L. Book, J. P. Boris and K. Hain, J. Comp. Phys. 18, 248 (1975).

8. S. T. Zalesak, J. Comp. Phys. 31, 335 (1979).

9. J. U. Brackbill and D. W. Forslund, to appear in the J. Comp. Phys. and D. W. Forslund and J. U. Brackbill, to appear in Phys. Rev. Lett.

10. D. W. Forslund, J. M. Kindel and K. Lee, Phys. Rev. Lett. 39, 385 (1977).

11. R. Jones, private communication.

12. S. I. Braginskii, Rev. Plasma Phys. 1, 205 (1965).

13. F. Harlow, recommended in private communication.

14. L. G. Spitzer, Physics of Fully Ionized Gases, John Wiley, New York (1962).

15. J. Denavit, J. Comp. Phys. 42, (1981).

16. R. J. Mason, Phys. Fluids 14, 1943 (1971).

Figure 1. Tests of suprathermal transport through a fixed ion background.

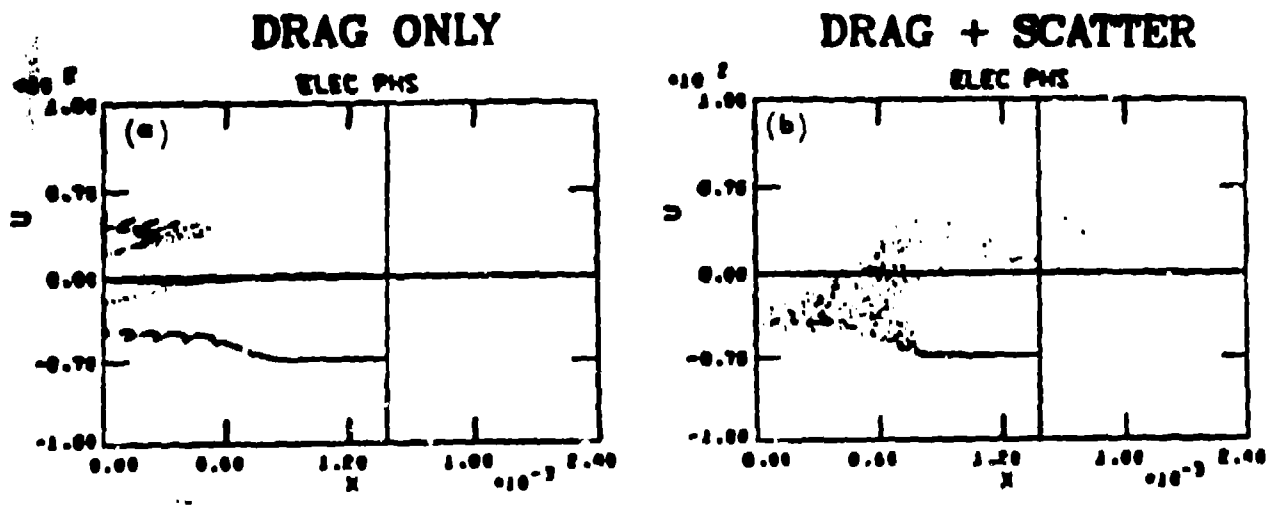

**********DRAG + SCATTER + E-FIELD **********

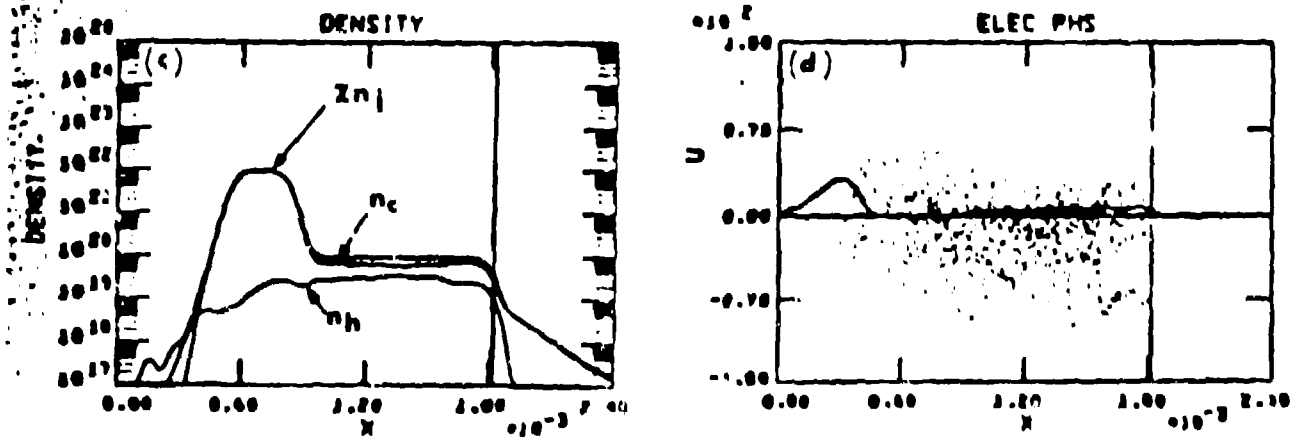

Figure 2. A foil exposed to 35 keV emission. (a) and (b) no scatter and no drag, (b) and (e) scatter only, (d) and (f) scatter plus drag.

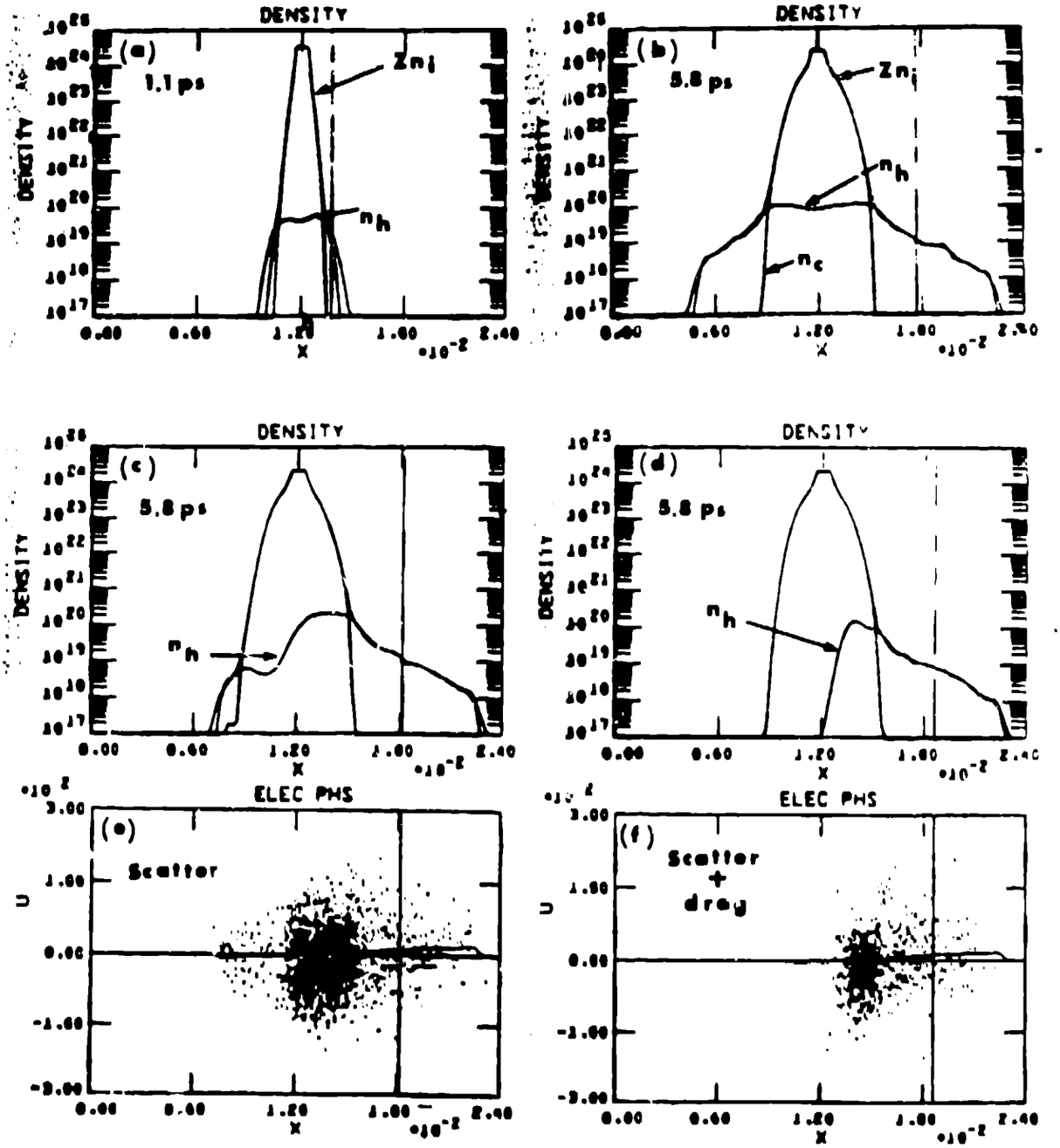

Figure 3. 150 keV suprathermal transport through a 4.8 μm foil, initially with $T_c = T_i = 1$ eV.

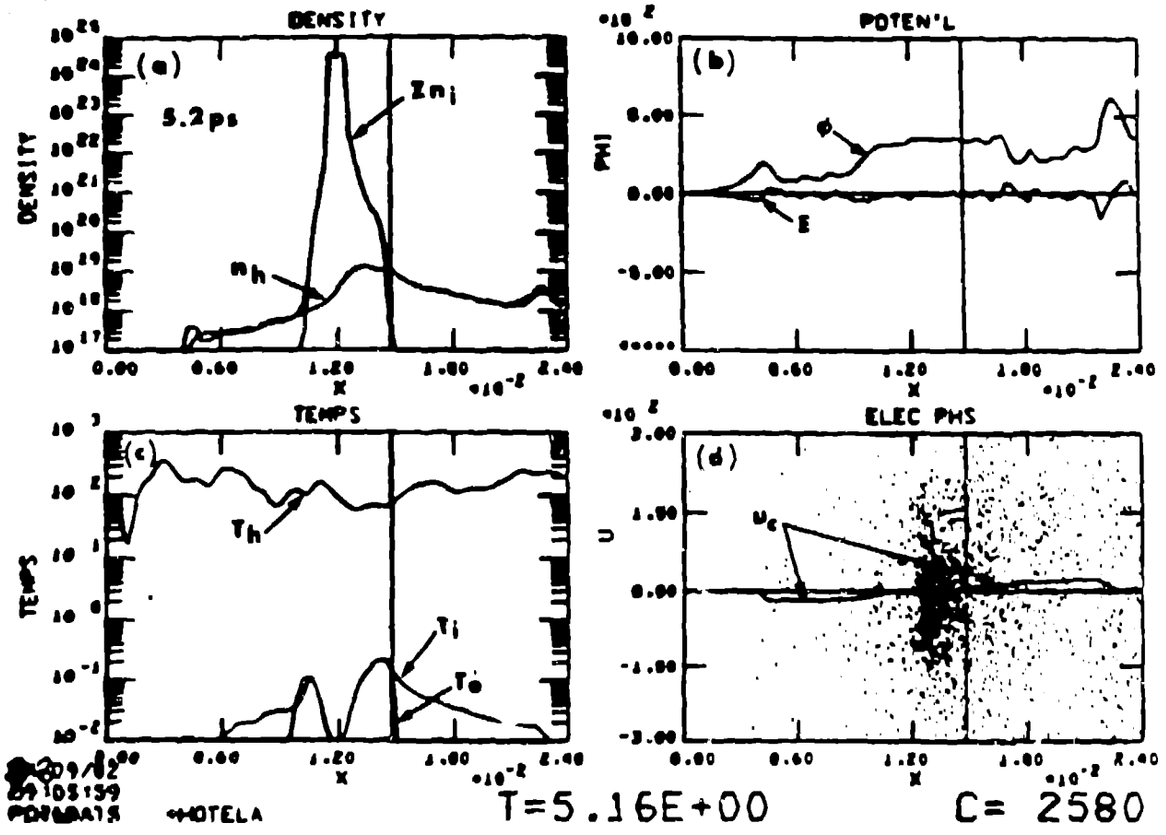

Figure 4. The closure of a vacuum gap.